

Searching for an elusive charged Higgs at the Large Hadron Collider

Ushoshi Maitra,^{1,*} Biswarup Mukhopadhyaya,^{1,†}

S. Nandi,^{2,‡} Santosh Kumar Rai,^{1,§} and Ambresh Shivaji^{1,¶}

¹*Regional Centre for Accelerator-based Particle Physics,*

Harish-Chandra Research Institute,

Chhatnag Road, Jhusi, Allahabad 211019, India

²*Department of Physics and Oklahoma Center for High Energy Physics,*

Oklahoma State University, Stillwater OK 74078-3072, USA

(Dated: January 9, 2014)

Abstract

We study the signals for a "fermiophobic" charged Higgs boson present in an extension of the standard model with an additional Higgs doublet and right handed neutrinos, responsible for generating Dirac-type neutrino masses. We study the pair production of the charged Higgs at the Large Hadron Collider (LHC), which can be relatively light and still allowed by experimental data. The charged Higgs decays dominantly into a W boson and a very light neutral scalar present in the model, which decays invisibly and passes undetected. We find that the signal for such a charged Higgs is overwhelmed by the standard model background and will prove elusive at the 8 TeV run of the LHC. We present a cut-flow based analysis to pinpoint a search strategy at the 14 TeV run of the LHC which can achieve a signal significance of 5σ for a given mass range of the charged Higgs.

Keywords: Charged Higgs, LHC, Neutrino mass.

* Email: ushoshi@hri.res.in

† Email: biswarup@hri.res.in

‡ Email: s.nandi@okstate.edu

§ Email: skrai@hri.res.in

¶ Email: ambreshkshivaji@hri.res.in

I. INTRODUCTION

The search for new physics beyond the standard model is continuing at the Large Hadron Collider (LHC). Although we are yet to see any clear hint, there is reason for exhilaration in another way, namely, the discovery of a boson of mass ~ 125 GeV [1]. The properties of this particle are very similar to the Higgs boson predicted in the standard model (SM), but possibilities of some new physics information contained in it cannot yet be ruled out. Thus a great deal of attention has shifted to the exploration of physics beyond the standard model (BSM) in the electroweak symmetry breaking sector.

One vexing issue, often mentioned as a motivation for BSM physics, is the identification of a mechanism for neutrino mass generation. This basically means finding some explanation for the smallness of neutrino masses as compared to those for the other fermions, and also the very different nature of mixing evinced in the neutrino (or more precisely, lepton) sector [2]. It is thus natural that efforts to unravel new physics in the Higgs sector will sometimes be guided by considerations related to neutrino masses [3–6]. The LHC signals of any scenario proposed in this context are also of undeniable interest [7, 8].

In this paper, we consider a model which not only accounts for the tiny neutrino masses, but also plays a role in the electroweak symmetry breaking mechanism. We are interested in a two Higgs doublet model with right-handed neutrinos proposed by Gabriel and Nandi [4]. The essential idea is that neutrinos, like all other fermions, have Dirac masses, but are much lighter than the others because their masses come from a different Higgs doublet. The Yukawa couplings of the neutrinos can still be $\mathcal{O}(1)$. This is ensured by giving a very tiny vacuum expectation value (vev) \sim eV to the neutral component of one of the Higgs doublets, which due to a Z_2 symmetry couples only with the neutrino sector. The charged Higgs in this model therefore has very different properties when compared to other standard two Higgs doublet models (2HDM) [9]. It is found to couple very weakly with the quarks while a large coupling with charged leptons and right-handed neutrinos is allowed. Thus, the leptonic mode is the most promising decay channel of this charged Higgs for $\mathcal{O}(1)$ Yukawa couplings in the neutrino sector [7]. Depending upon the mass of the charged Higgs other decay modes are also possible. In a similar model proposed by Davidson and Logan [6, 8], which considers a $U(1)$ global symmetry in place of the discrete Z_2 symmetry, only

leptonic decay modes of the charged Higgs were allowed.

The branching probabilities for the decay of the charged Higgs are very sensitive to the small vev of the additional doublet, which couples to the neutrinos [7]. As recent astrophysical bounds on the neutrino Yukawa couplings in such extensions of the SM suggest that the vev of the second doublet cannot be in the sub-eV range [6, 10], the charged Higgs can no longer decay dominantly into a leptonic final state. It turns out that the main decay mode for the charged Higgs is into a W boson and a light neutral scalar present in the model. In this work we mainly focus on the challenges presented for a charged Higgs search at the LHC, when it decays through the W mode. We study the pair production of the charged Higgs at the LHC and consider its decay to W boson and the neutral scalar. The signal is identified by two isolated leptons and a large missing energy. We have analyzed the most dominant SM background subprocesses that affect the signal, to estimate the signal significance. The study is carried out at both the 8 TeV and 14 TeV center-of-mass energies for the LHC. We find that it is practically impossible to achieve any significant signal for the charged Higgs in this model with the available integrated luminosity at 8 TeV. The situation is much more optimistic at 14 TeV, if one waits for a sizeable luminosity to accumulate. There, on applying appropriate kinematical event selection procedure, a signal significance of 5σ at 14 TeV can be reached with an integrated luminosity of 4000 fb^{-1} for $M_{H^\pm} = 150 \text{ GeV}$. The observation of the signal is found to be more promising for heavier charged Higgs masses.

The paper is organized as follows. In Section II we describe the model briefly. Various constraints on the model parameters are discussed in Section III. In Section IV, we discuss the charged Higgs pair production and major backgrounds for the signal at the LHC. Results are presented in Section V and we conclude in Section VI.

II. A BRIEF REVIEW OF THE MODEL

The model under consideration is based on the symmetry group $\mathcal{G}_{SM} \times Z_2$, where $\mathcal{G}_{SM} \equiv SU(3)_c \times SU(2)_L \times U(1)_Y$. In addition to the matter fields in the SM, the model includes two scalar doublets χ and ϕ , and three $SU(2)_L$ singlet right-handed neutrinos ν_R^i , $i = 1, 2, 3$. All the SM fermions and the scalar doublet χ are even under the discrete symmetry Z_2 ,

while the right-handed neutrinos and the scalar doublet ϕ are odd under Z_2 . The most general scalar potential and the Yukawa interaction of leptons with the scalar doublets which respect the $\mathcal{G}_{SM} \times Z_2$ symmetry are [4],

$$\mathcal{V} = -\mu_1^2 \chi^\dagger \chi - \mu_2^2 \phi^\dagger \phi + \lambda_1 (\chi^\dagger \chi)^2 + \lambda_2 (\phi^\dagger \phi)^2 + \lambda_3 (\chi^\dagger \chi)(\phi^\dagger \phi) - \lambda_4 |(\chi^\dagger \phi)|^2 - \frac{1}{2} \lambda_5 [(\chi^\dagger \phi)^2 + (\phi^\dagger \chi)^2], \quad (1)$$

$$\mathcal{L}_Y = y_l^{ij} \bar{\Psi}_L^{l,i} l_R^j \chi + y_{\nu_l}^{ij} \bar{\Psi}_L^{l,i} \nu_R^j \tilde{\phi} + h.c., \quad (2)$$

where, $\bar{\Psi}_L^{l,i} = (\bar{\nu}_l^i, \bar{l}^i)_L$ and l_R^j are the usual $SU(2)_L$ lepton doublet and singlet fields, respectively and y_f^{ij} ($f \equiv l, \nu_l$) represent the matrix elements of the lepton Yukawa matrices. The standard electroweak symmetry is broken spontaneously by giving a vev, $V_\chi \simeq 246$ GeV to the χ doublet, while the Z_2 symmetry is broken by a vev, V_ϕ for the ϕ doublet. The spontaneous breaking of the Z_2 symmetry is arranged for generating small neutrino masses, $m_{\nu_l} \sim V_\phi$ which can be in the sub-eV/eV range for $\mathcal{O}(1)$ Yukawa couplings. We note that we are assuming lepton number conservation so that the Majorana mass terms for the right handed neutrinos, ν_R , $M \nu_R^T C^{-1} \nu_R$ are not allowed. Thus the light left-handed neutrinos cannot acquire masses via the usual see-saw mechanism [11]. Dirac mass, as obtained from Eq. 2 from the tiny vev of ϕ is the only possibility.

As a result of the symmetry breaking, the physical Higgs sector includes charged scalars H^\pm , two neutral CP-even scalars h and σ and a neutral pseudoscalar ρ . The masses for these particles are given by,

$$\begin{aligned} M_{H^\pm}^2 &= \frac{1}{2}(\lambda_4 + \lambda_5)V^2, & M_\rho^2 &= \lambda_5 V^2 \\ M_h^2 &= 2\lambda_1 V_\chi^2, & M_\sigma^2 &= 2\lambda_2 V_\phi^2, \end{aligned} \quad (3)$$

where, $V^2 = V_\chi^2 + V_\phi^2$. We have neglected the subdominant terms in V_ϕ when deriving these relations. We note that in the case of exact Z_2 symmetry, the σ will be exactly massless. The breaking of this Z_2 symmetry with a tiny vev V_ϕ gives mass to the σ , as well as tiny Dirac masses to the observed neutrinos. Therefore in this model, the neutral scalar field σ is very light and the field h behaves like the SM Higgs boson. The CP-even scalars (h, σ) are the mass eigenstates and they are related to the weak eigenstates (h_0, σ_0) by the mixing angle θ :

$$h = h_0 \cos \theta - \sigma_0 \sin \theta, \quad \sigma = h_0 \sin \theta + \sigma_0 \cos \theta. \quad (4)$$

where,

$$\cos \theta = 1 + \mathcal{O}(V_\phi^2/V_\chi^2), \quad \sin \theta = -\frac{\lambda_3 - \lambda_4 - \lambda_5}{2\lambda_1} \left(\frac{V_\phi}{V_\chi} \right) + \mathcal{O}(V_\phi^2/V_\chi^2). \quad (5)$$

This mixing can be neglected because $V_\phi \ll V_\chi$. It is also clear from the above equations that M_ρ lies around the electroweak scale.

In the lepton Yukawa sector the above symmetry breaking leads to neutrino masses given by, $m_{\nu_a} = y_\nu^a V_\phi / \sqrt{2}$, where y_ν^a are the eigenvalues of the neutrino Yukawa matrix. The Yukawa interaction of the charged Higgs with the leptons can then be written down following Eq. 2 as,

$$\mathcal{L}_Y \supset y_\nu^a \frac{V_\chi}{V} U_{ia} \bar{l}_L^i \nu_R^a H^- + y_l^i \frac{V_\phi}{V} U_{ia} \bar{l}_R^i \nu_L^a H^- + h.c. \quad (6)$$

In the above equation, i represents the flavour index while a is the index representing neutrino components in mass eigenstate. The $y_l^i = \sqrt{2}m_l^i/V_\chi$ are the charged lepton Yukawa couplings while U_{ia} represent the elements in the PMNS matrix [12] for the mixing of the neutrino flavours.¹ Note that the second term in Eq. 6 is clearly sub-dominant and negligible (suppressed by the factor V_ϕ/V) when compared to the first term and can therefore be safely neglected when considering the interaction strength of the charged Higgs with the leptons. As the couplings of charged Higgs with SM quarks are also generated through terms similar to the second term in Eq. 6, the charged Higgs is very weakly coupled to quarks and in all practicality behaves as a "chromophobic" field. This property of the charged Higgs plays a crucial role in avoiding strong constraints on its mass, otherwise evident in other 2HDM, from low energy physics experiments such as weak meson decays and mixing. Thus in the Yukawa sector, only the decay $H^\pm \rightarrow l_L^\pm \nu_R$ becomes relevant. Other main decay modes of the charged Higgs include $H^\pm \rightarrow W^\pm \sigma$ and $H^\pm \rightarrow W^\pm \rho$ which have gauge coupling interaction strengths. The branching ratios of charged Higgs decay is quite sensitive to the value of V_ϕ . As the leptonic channel ($l \nu_l$) is dictated by the coupling strength given by $\sim m_\nu/V_\phi$ (see Eq. 6), smaller values of V_ϕ for a fixed neutrino mass increase the branching probability. To highlight this, we consider two sets of values for V_ϕ and show the branching probabilities of the charged Higgs decay as a function of its mass in Fig. 1. Note that

¹ $\nu^i = \sum_a U_{ia} \nu^a$.

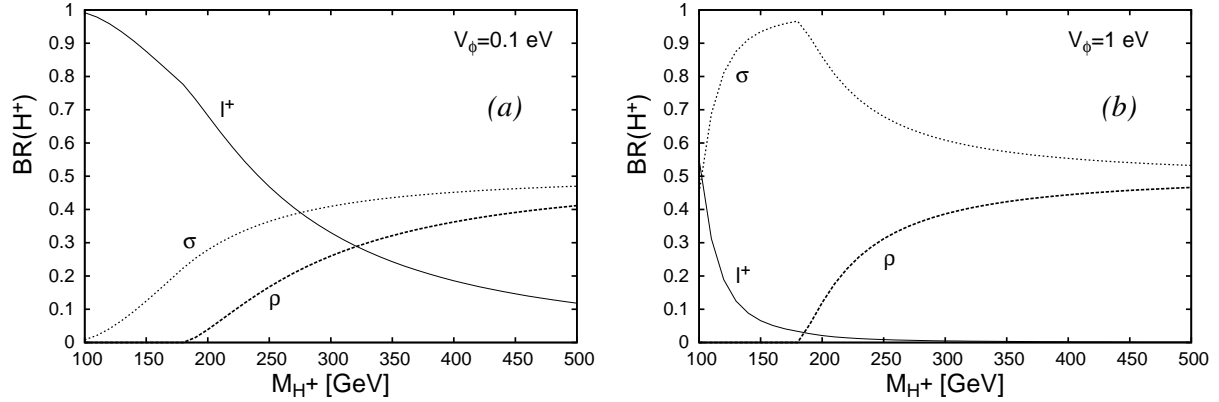


FIG. 1. Charged Higgs branching ratios as function of its mass for (a) $V_\phi = 0.1$ eV and (b) $V_\phi = 1$ eV. The mass of σ particle is related to V_ϕ as in Eq. 3. We have chosen the other relevant variables $\lambda_2 = 1.0$ and $M_\rho = 100$ GeV for calculating the above branching ratios.

the neutrino data as shown in Table I have been incorporated when calculating the partial decay widths of the charged Higgs decaying into the three generations of leptons. If V_ϕ is in the sub-eV range as shown in Fig. 1a, it is found to decay mostly through the leptonic mode for $M_{H^\pm} \leq 200$ GeV, while if V_ϕ is increased to about an eV (Fig. 1b), it decays dominantly into $W^\pm\sigma$. As the value of V_ϕ is increased further, we find that the leptonic channel becomes completely negligible and the $W^\pm\sigma$ becomes the only significant mode available for the charged Higgs decay for $M_{H^\pm} \leq 200$ GeV.

III. CONSTRAINTS ON MODEL PARAMETERS

As the model under consideration is quite different from the generic 2HDM and is envisioned to account for the observed neutrino masses and mixing angles, it becomes imperative to first check how the experimental constraints affect the parameters of the model. A brief discussion on several constraints on the model parameters is already present in Ref. [4]. We choose to accommodate them with new and updated results that have modified these constraints as well as supplement them with additional constraints, if any.

We acknowledge that any scenario explaining neutrino masses will also need to address their mixing, and reproduce the form of the PMNS matrix as suggested by various obser-

Parameters	NH	IH
$\sin^2\theta_{12}$	$0.307^{+0.052}_{-0.048}$	$0.307^{+0.052}_{-0.048}$
$\sin^2\theta_{23}$	$0.386^{+0.055}_{-0.251}$	$0.392^{+0.057}_{-0.271}$
$\sin^2\theta_{13}$	$2.41^{+0.72}_{-0.72} \times 10^{-2}$	$2.42^{+0.73}_{-0.71} \times 10^{-2}$
$m_{\nu_2}^2 - m_{\nu_1}^2$	$7.54^{+0.55}_{-0.64} \times 10^{-5} \text{eV}^2$	$7.54^{+0.55}_{-0.64} \times 10^{-5} \text{eV}^2$
$m_{\nu_3}^2 - \frac{1}{2}(m_{\nu_1}^2 + m_{\nu_2}^2)$	$2.43^{+0.24}_{-0.19} \times 10^{-3} \text{eV}^2$	$-2.42^{+0.25}_{-0.19} \times 10^{-3} \text{eV}^2$

TABLE I. Neutrino mass-mixing parameters with 3σ uncertainties [13]. The allowed ranges of parameters for the Normal Hierarchy (NH) and Inverted Hierarchy (IH) cases are shown separately.

variations [13]. The PMNS matrix is parameterized by three mixing angles and can have one phase whose value is yet unknown. The current values of these angles and the neutrino mass-squared differences are shown in Table I. From the measurements on the neutrino mass-squared differences we can conclude that in both the normal and inverted hierarchy scenarios, the mass of the heaviest neutrino is $\gtrsim 0.05$ eV. We have already discussed the sensitivity of the branching ratios of the charged Higgs to the magnitude of V_ϕ . Clearly, from neutrino data, one is free to choose $\mathcal{O}(1)$ Yukawa couplings (y_ν). However, the right-handed neutrinos are new relativistic degrees of freedom present in our model. Due to its coupling with the charged Higgs and the leptons, they should be excessively produced in the early Universe, for example, via the charged Higgs mediated t -channel process $l^+l^- \leftrightarrow \nu_R\bar{\nu}_R$. We can therefore put a constraint on the neutrino Yukawa coupling using the big-bang nucleosynthesis (BBN) bound on new relativistic degrees of freedom (δN_ν) [14]. The latest results combining Planck, WP, Baryon Acoustic Oscillation (BAO) and high multipole CMB data, on the upper limit of extra relativistic degrees of freedom give $\delta N_{\nu,max} \simeq 1.0$ at 95% confidence level [15]. This bound can be translated into an upper bound on the neutrino Yukawa coupling or a lower bound on V_ϕ for a given neutrino mass which is given by [6]

$$V_\phi \gtrsim 60 m_{\nu_i}(|U_{li}|) \frac{100 \text{ GeV}}{M_{H^+}}. \quad (7)$$

The lower bound on V_ϕ is derived for the most massive neutrino labeled by l in U_{li} . The hierarchy in the neutrino masses is therefore not important here. We have considered the maximal mixing for which $|U_{li}| \simeq 1/\sqrt{2}$. A value of U_{li} consistent with the neutrino data

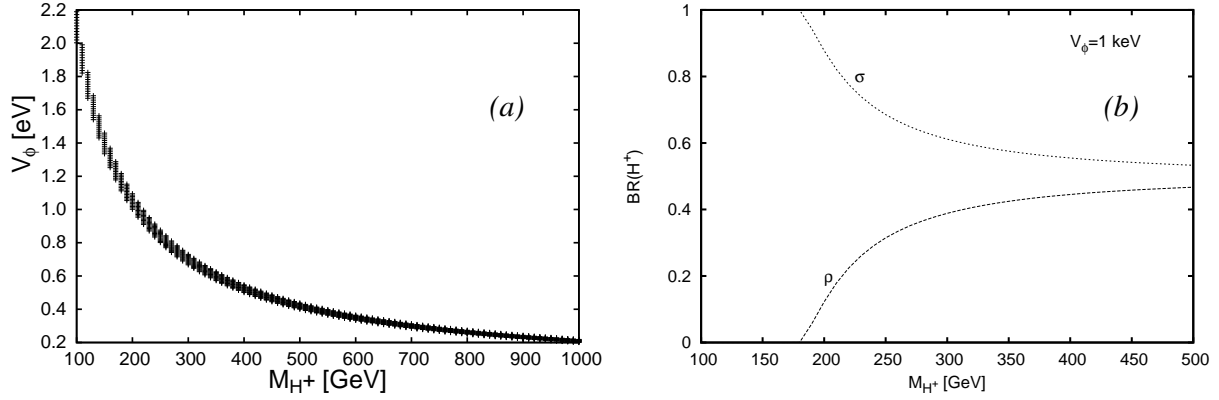


FIG. 2. (a) The variation of the lower bound on V_ϕ as a function of M_{H^+} as defined by Eq. 7. The band represents the 3σ uncertainties shown in Table I. (b) The branching ratios of the charged Higgs decay for the choice of $V_\phi = 1$ keV.

does not alter the numerical value of the bound significantly. If $M_{H^\pm} \sim 100$ GeV, the above bound implies $V_\phi \gtrsim 2$ eV. In Fig. 2a, we have shown the variation of the lower bound on V_ϕ as a function of M_{H^\pm} consistent with the neutrino data. For a fixed value of M_{H^\pm} , the range of V_ϕ illustrates 3σ uncertainty in neutrino data. This, when considered with the decay properties of the charged Higgs illustrated in Fig. 1 shows that for a light charged Higgs (100-200 GeV), the dominant decay is to $W\sigma$ as $V_\phi > 1$ eV.

In addition to that, if the supernova neutrino observations and the energy-loss argument for supernova cores are also considered, the lower bound on V_ϕ can be pushed to $V_\phi \gtrsim 1$ keV [10]. This also takes care of the excessive production of neutrinos through the σ boson mediated process $\nu_i + \bar{\nu}_i \rightarrow \nu_j + \bar{\nu}_j$, in the early Universe. Since $\Gamma(H^\pm \rightarrow l_L^\pm \nu_R) \propto m_\nu^2/V_\phi^2$, the leptonic decay mode of the charged Higgs will be extremely suppressed as the Yukawa couplings are further suppressed ($y_\nu \sim m_\nu/V_\phi$). Instead, it will decay overwhelmingly via the modes $H^\pm \rightarrow W^\pm \sigma$ and $W^\pm \rho$ (see Fig. 2b), thus behaving more like a "fermiophobic" field.

The values of coupling parameters $\lambda_1, \lambda_2, \lambda_4$ and λ_5 appearing in the scalar potential (Eq. 1) can be fixed once we make a choice for the scalar masses M_h, M_σ, M_ρ and M_{H^\pm} (see Eq. 3). To incorporate the recently discovered SM-like Higgs boson in our model, we would like to have $M_h \sim 125 - 126$ GeV, which fixes λ_1 . We can choose any value for λ_2

which is not very large so that $M_\sigma \simeq V_\phi \sim \text{keV}$. Note that a 1 keV σ particle will decay into neutrinos in about 10^{-9} seconds. Although $\mathcal{O}(1)$ values of λ_3 do not affect the scalar mass spectrum, it appears in various interaction vertices. We find that by choosing $\lambda_3 = \lambda_4 + \lambda_5$ we can suppress large contributions to the invisible decay width of the SM-like Higgs via the decay mode $h \rightarrow \sigma\sigma$. As the present LHC data allows a maximum of 20% branching ratio for any invisible decay mode(s) of the Higgs boson at the 95 % C.L. [16, 17], allowing $BR(h \rightarrow \sigma\sigma) = 20\%$ puts a condition on λ_3 which is given by,

$$\begin{aligned}\lambda_3 &= 0.0133 + \lambda_5 + \lambda_4, \\ &= 0.0133 + 0.3305 \times \left(\frac{M_{H^\pm}}{100 \text{ GeV}} \right)^2,\end{aligned}\tag{8}$$

where we have used Eq. 3 and $V \simeq V_\chi = 246 \text{ GeV}$. Even with the above choice of λ_3 , a light enough ρ may further contribute to the Higgs invisible decay width. We may therefore choose M_ρ sufficiently large so that this situation is avoided. The pseudoscalar ρ , belonging to the doublet ϕ has no significant interaction with charged leptons and quarks, and decays mostly into a neutrino-antineutrino pair. Since the decay $Z \rightarrow \rho\sigma$ contributes to the invisible decay width of the Z boson, the experimental measurements require $M_\rho \gtrsim 78 \text{ GeV}$ [18]. When $M_\rho > m_Z$ one also needs to consider the LEP2 data for the signal from the process $e^+e^- \rightarrow Z^* \rightarrow \rho\sigma$. Non observation of any such signal puts a lower bound on the ρ mass of 95 GeV [4]. Note that if we take $M_\rho = 100 \text{ GeV}$, $\Gamma(h \rightarrow \rho\rho^*) \sim \text{eV}$ which will have negligible contribution to the Higgs invisible decay width.

The only bound on the mass of the charged Higgs in our model comes from the direct searches for the pair production at the LEP experiments. Due to very suppressed coupling of the charged Higgs with the quarks, the constraints from rare processes such as $b \rightarrow s\gamma$ do not put any additional bound on the charged Higgs mass. Thus it is enough to have $m_{H^\pm} \geq 79.3 \text{ GeV}$ [18].

IV. PROSPECTS OF THE CHARGED HIGGS AT THE LHC: SIGNAL BACKGROUND ANALYSIS

Since the chromophobic nature of the charged Higgs in this scenario disallows its production in association with a top (anti-top) quark, one has to rely on electroweak sub-processes

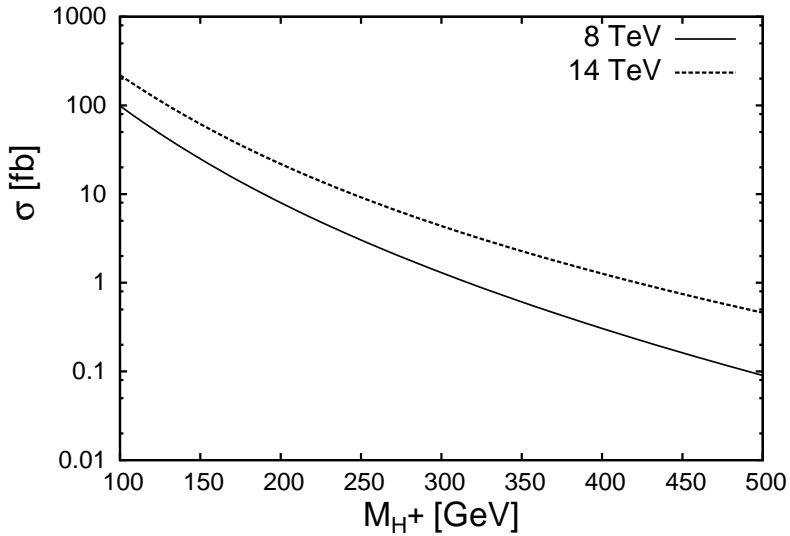


FIG. 3. Charged Higgs pair production cross section as function of charged Higgs mass at 8 TeV and 14 TeV LHC center-of-mass energies.

for its pair production. Thus the H^\pm pair is produced via Drell-Yan process through the exchange of photon and Z boson in the s-channel. It can also be produced at the LHC through vector boson fusion (VBF), namely, $qq \rightarrow qqV^*V^* \rightarrow qqH^+H^-$ where $V = \gamma, Z, W^\pm$. However, the VBF production cross section is quite suppressed when compared to Drell-Yan. The pair production cross section for the charged Higgs at the LHC at center-of-mass energies of 8 TeV and 14 TeV is shown in Fig. 3. The cross sections have been computed using CTEQ6L1 parton distribution functions (PDFs) [19]. Since the coupling of SM-like Higgs boson with the charged Higgs is not negligible, the charged Higgs pair production may also receive additional contributions via a Higgs (h) mediated gluon fusion process. For our choice of λ_3 and $M_{H^\pm} = 150$ GeV, the $gg \rightarrow h^* \rightarrow H^+H^-$, we find the gluon mediated cross section is about 1.86 fb for the 14 TeV run of the LHC. For larger values of M_{H^\pm} , one expects this contribution to grow, as λ_3 also increases (Eq. 8). But the s-channel mediated process receives a significant propagator suppression (as the effective $\hat{s} > 2M_{H^\pm}$ for pair production), making it quite small for larger M_{H^\pm} .

The charged Higgs can also be produced singly in association with a ρ or σ in the channel $qq' \rightarrow \rho H^\pm, \sigma H^\pm$. These production modes lead to single H^\pm along with large missing energy when ρ and σ decay to $\nu\bar{\nu}$. Although the rate of single charged Higgs production

is comparable to that of pair produced charged Higgs, the single- W^\pm background is very large compared to that from W^+W^- . So we study the signals for the charged Higgs via pair production. As illustrated in Fig. 2b when $V_\phi \sim \text{keV}$, $H^\pm \rightarrow W^\pm \sigma$ is the most favourable decay channel as compared to other decays. As σ decays to neutrinos with 100% branching probability, we will be focusing on events with large transverse missing energy (\cancel{E}_T). The W produced from the charged Higgs, decays into $(l \nu_l)$. Thus, the signature of charged Higgs in this model is $pp \rightarrow H^+H^- \rightarrow W^+W^- \sigma\sigma \rightarrow l^+l^- + \cancel{E}_T$.

For our analysis, we have used the package **MadGraph 5** [20] to generate events for the signal as well as the SM background processes. To generate the events for the signal, we have included the interaction vertices of the new model in **MadGraph 5** using the publicly available package **Feynrules** [21]. We have kept the factorization and renormalization scales same as the default event-by-event **MadGraph 5** value which happens to be the transverse mass of the pair produced particle [22]. A full simulation of the generated events has been carried out by including fragmentation and hadronization effects using **PYTHIA 8** [23]. We also include the initial and final state radiations. In order to get a real assessment of the signal and the background at the detector level we have considered isolated leptons and jets. The event selection criteria that we use is consistent with that of the ATLAS detector [24]. However, a 100% lepton identification (for e and μ) efficiency is assumed. To account for the detector resolutions we have smeared the energies/transverse momenta of leptons and jets with Gaussian functions as shown in Table II [25].

The model parameters used in our analysis are

$$\begin{aligned}
\lambda_1 &= 0.13, & \lambda_2 &= 1.0, & \lambda_3 &= 0.0133 + \lambda_4 + \lambda_5, \\
\lambda_4 &= 2\frac{M_{H^+}^2}{V^2} - \lambda_5, & \lambda_5 &= \frac{M_\rho^2}{V^2}, & V_\phi &= 1 \text{ keV}, \\
M_\rho &= 100 \text{ GeV}, & M_\sigma &= \sqrt{2}V_\phi, & M_h &= 126 \text{ GeV}.
\end{aligned} \tag{9}$$

It is worth pointing out that we have chosen neutrino masses (normal hierarchy) which are consistent with the neutrino data. In our analysis, however, neutrino masses and their hierarchy are of no consequence because the leptonic decay mode of the charged Higgs for $V_\phi = 1 \text{ keV}$ is highly suppressed. The major subprocesses in the SM that contribute as background to our signal are $pp \rightarrow t\bar{t}$, W^+W^- , ZZ and also $pp \rightarrow h \rightarrow WW^*/ZZ^*$.

	Electrons $\frac{\sigma(E)}{E}$	Muons $\frac{\sigma(p_T)}{p_T}$	Jets $\frac{\sigma(E)}{E}$	Uncl. Energy $\sigma(E)$
Formula	$\frac{a}{\sqrt{E}} \oplus b \oplus \frac{c}{E}$	a if $p_T < 100$ else $a + b \log(\frac{p_T}{100})$	$\frac{a}{\sqrt{E}} \oplus b \oplus \frac{c}{E}$	$\alpha \sqrt{\sum_i E_T^{uncl}}$
$ \eta < 1.5$	$a = 0.11, b = 0.007,$ $c = 0.25$	$a = 0.02, b = 0.08$	$a = 0.65, b = 0.027,$ $c = 4$	$\alpha = 0.55$
$1.5 < \eta < 2.5$	$a = 0.13, b = 0.007,$ $c = 0.25$	$a = 0.03, b = 0.06$	$a = 1.10, b = 0.01,$ $c = 6.5$	$\alpha = 0.55$
$2.5 < \eta < 3.0$	—	—	$a = 1.10, b = 0.01,$ $c = 6.5$	$\alpha = 0.55$
$3.0 < \eta < 4.5$	—	—	$a = 1.00, b = 0.05,$ $c = 1.0$	$\alpha = 0.55$

TABLE II. Functional form and parameters of the resolution functions of different physics objects. These parameterizations give the value of σ parameter of the gaussian functions used. The first and second column of the last two rows are kept blank as the leptons are identified within $|\eta| < 2.5$.

Note that we have identified the Higgs (h) mediated subprocesses separately. As the Higgs production through gluon-fusion is a loop mediated process, we have included it in **Madgraph 5** via an effective operator. The $t\bar{t}$ background is a reducible background which can be ignored by selecting zero jet events. By removing the Z -peak (selecting a narrow window of 30 GeV around the peak in the invariant mass distribution of the dileptonic system) we can also suppress the ZZ background. This invariant mass cut partially takes care of the $pp \rightarrow h \rightarrow ZZ^*$ background when the on-shell Z decays into charged lepton pair. As we shall explain in the next section, a large missing transverse energy (\cancel{E}_T) cut is essential for our signal-background analysis. We find that on applying a large \cancel{E}_T cut the $pp \rightarrow h \rightarrow WW^*/ZZ^*$ backgrounds become negligible. Thus the $pp \rightarrow W^+W^-$ is the major irreducible background to our signal.

Note that we have performed a leading order analysis here. Since the production of the charged Higgs takes place via a Drell-Yan process, QCD corrections are not expected

to make any significant difference to the kinematic distributions, to be discussed later, on which our conclusions hinge so crucially.

V. RESULTS

In this section, we present our results for charged Higgs masses of 150 GeV and 200 GeV as benchmark values. For $M_{H^\pm} = 150$ (200) GeV, the pair production ($pp \rightarrow H^+ H^-$) cross sections at 8 TeV and 14 TeV LHC center-of-mass energies are 21.48 (6.86) fb and 53.05 (18.73) fb respectively. The dominant decay mode of the charged Higgs for our choice of parameters is $W^\pm \sigma$. The branching fraction of this decay mode for the charged Higgs mass of 150 GeV is close to 100%. Since we have taken $M_\rho = 100$ GeV, for 200 GeV charged Higgs the $W^\pm \rho$ decay mode is also allowed and $H^\pm \rightarrow W^\pm \sigma$ branching probability reduces to about 88% (see Fig. 2b). Thus for the 200 GeV charged Higgs, $W\sigma$ mode still remains the most dominant channel. However, even the $W^\pm \rho$ mode might contribute to our signal, since the ρ can also decay invisibly. For $M_\rho = 100$ GeV, there are two possible decay modes, *viz.* $\rho \rightarrow Z\sigma$ and $\rho \rightarrow \nu\bar{\nu}$. But much like the charged Higgs, the choice of $V_\phi = 1$ keV suppresses the invisible decay of ρ and it decays to $Z\sigma$ with 100% branching probability. The decay of the charged Higgs is followed by the leptonic decay of W boson. Since we have isolated both the leptons and jets, the events with isolated jets are removed and we select the signal and background events consisting of two isolated charged leptons and missing energy.

The basic acceptance cuts for the signal as well as background include,

$$p_T^l > 20 \text{ GeV}, |\eta_l| < 2, \Delta R_{ll} > 0.4, |m_{ll} - m_Z| > 15 \text{ GeV and } \cancel{E}_T > 50 \text{ GeV.} \quad (10)$$

With these cuts at 8 TeV center-of-mass energy, the signal cross section for 150 GeV charged Higgs mass is quite small (~ 0.13 fb) whereas the background cross section is 64.12 fb. We note that the signal has additional sources of missing energy due to the presence of σ particles which completely decay to neutrinos. Thus, selecting events with high missing transverse energy is expected to be helpful in distinguishing the signal from the background. However, when the mass of charged Higgs is close to m_W the effect of large missing transverse energy cut is not very helpful. As the mass of the charged Higgs increases, the

fraction of events with higher transverse momentum (p_T) as well as higher missing transverse energy (\cancel{E}_T) is larger in the signal as compared to the background. Thus, the effect of harder missing energy cut becomes evident. This feature is illustrated in Fig. 4. The

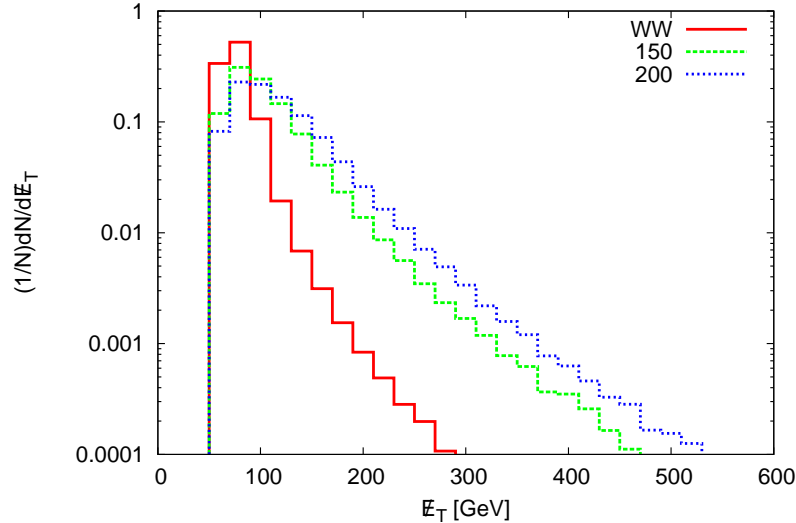


FIG. 4. A comparison of the missing energy distributions for the signal and the W^+W^- background at 8 TeV. Both the 150 GeV and 200 GeV charged Higgs mass cases of the signal is considered.

background, therefore, can be further reduced by raising the minimum missing energy cut. We find that the signal and background cross sections after applying 100 GeV minimum \cancel{E}_T cut become 0.04 fb and 2.11 fb respectively. This means, with the available luminosity of $\simeq 25 \text{ fb}^{-1}$ at 8 TeV, for one signal event the number of background events is about 52. Therefore, it is very difficult to see the signal excess over such a large background at the 8 TeV LHC. The situation gets worse for $M_{H^\pm} = 200$ GeV due to its smaller production cross section at 8 TeV. However, with larger center-of-mass energy (Fig. 3) there is a significant increase in the pair production cross section. At $\sqrt{s} = 14$ TeV the signal cross section is much larger and the data will be collected at much higher luminosity. Thus one expects to achieve greater signal significance at $\sqrt{s} = 14$ TeV run of the LHC.

The event selection criteria and basic acceptance cuts for the $\sqrt{s} = 14$ TeV analysis are kept same, as shown in Eq. 10. The cross sections for the $(2l + \cancel{E}_T)$ signal ($M_{H^\pm} = 150$ GeV) and background are respectively, 0.25 fb and 96.21 fb after applying the acceptance cuts. Motivated by the observation in the $\sqrt{s} = 8$ TeV analysis, we apply a minimum

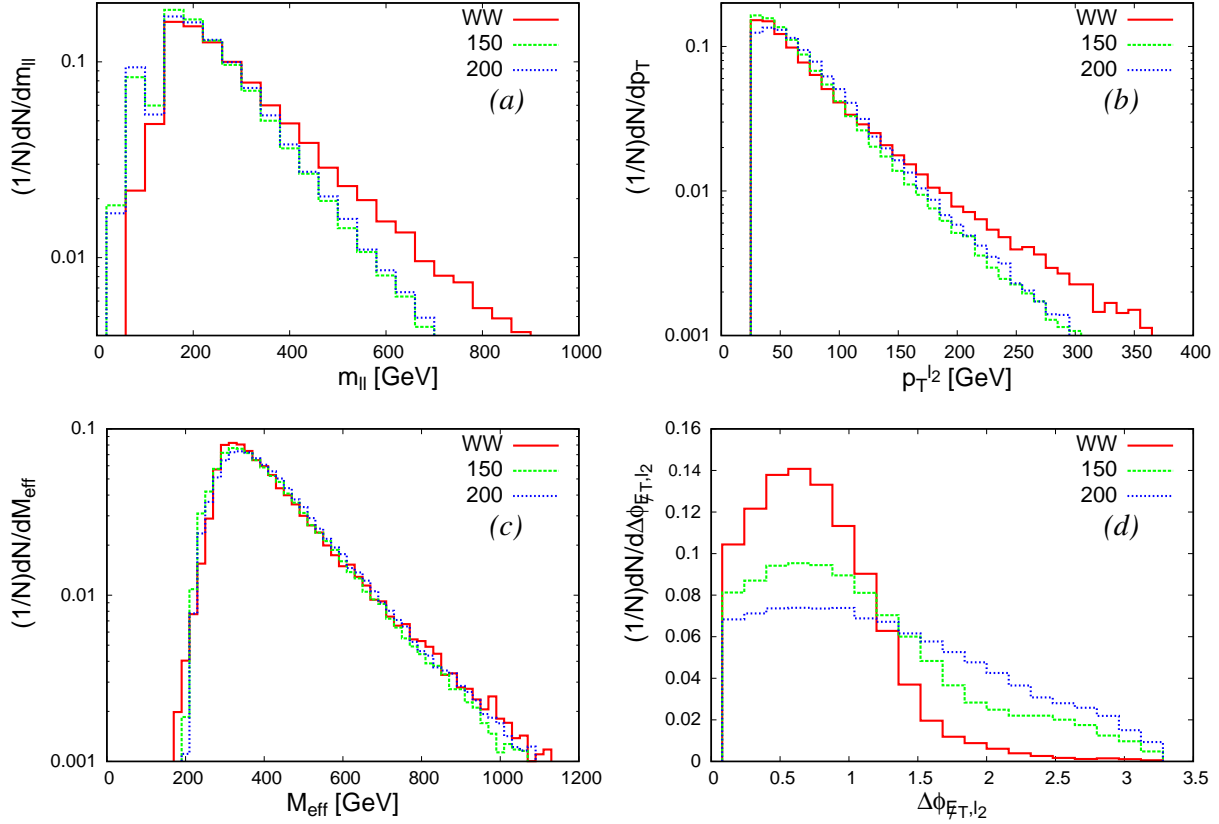


FIG. 5. Kinematic distributions for the $(2l + \cancel{E}_T)$ signal with $M_{H^\pm}=150, 200$ GeV and background (W^+W^-). The events satisfy the $\cancel{E}_T > 110$ GeV cut and the acceptance cuts listed in Eq. 10.

\cancel{E}_T cut of about 110 GeV to enhance the signal significance to ~ 2 . However, we note that raising the \cancel{E}_T cut beyond 110 GeV does not improve the situation and we need to construct suitable kinematic variables which can help in reducing the background further. In Fig. 5 we display kinematic distributions for the invariant mass (m_{ll}), the transverse momentum of the sub-leading lepton ($p_T^{l_2}$), the effective mass (M_{eff})² and the angle between the directions of missing energy and the subleading lepton in the transverse plane ($\Delta\phi_{\cancel{E}_T, l_2}$). These distributions are plotted after applying the large \cancel{E}_T cut. Quite clearly, it is the angle $\Delta\phi_{\cancel{E}_T, l_2}$ (Fig. 5d) which turns out to be the most effective kinematic variable in separating the signal from the background. We also note that this cut is more promising for the $M_{H^\pm} = 200$ GeV. Based on this we have applied a minimum cut of 1.6 on the angle

² $M_{eff} = \sum p_T^{visible} + \sum p_T^{missing}$

$\Delta\phi_{\cancel{E}_T, l_2}$. This improves the signal-to-background ratio significantly.

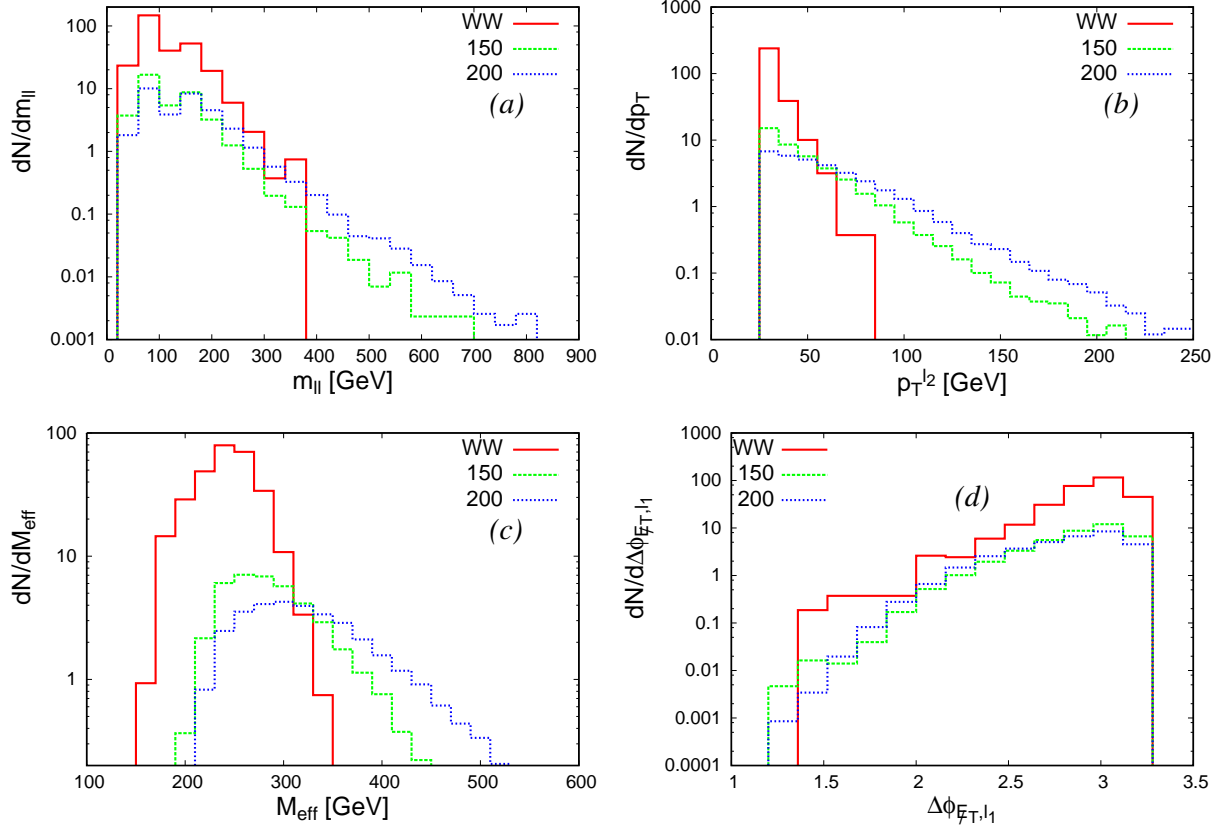


FIG. 6. Kinematic distributions for the $(2l + \cancel{E}_T)$ signal with $M_{H^\pm}=150, 200$ GeV and background (W^+W^-). The events satisfy the $\Delta\phi_{\cancel{E}_T, l_2} > 1.6$, $\cancel{E}_T > 110$ GeV cut and the acceptance cuts listed in Eq. 10.

The kinematic distributions shown in Fig. 6 have been plotted after applying the $\Delta\phi_{\cancel{E}_T, l_2}$ cut. If we compare the distributions for m_{ll} , $p_T^{l_2}$ and M_{eff} in Fig. 5 after the application of $\Delta\phi_{\cancel{E}_T, l_2}$ cut, as shown in Fig. 6, we find that this cut affects the background events quite significantly. In our case, the additional source of missing energy reduces the correlation between the leptons and the \cancel{E}_T , which is so crucially present in the W^+W^- background. This causes events of background events with high p_T to be removed once the above azimuthal angle cut is applied. We can see from these distributions that the cut on the angle $\Delta\phi_{\cancel{E}_T, l_2}$ followed by a suitable cut on $p_T^{l_2} / M_{eff}$ looks very promising in enhancing the signal significance. The kinematic distribution displayed in Fig. 6d indicates that a

minimum cut on $\Delta\phi_{\cancel{E}_T, l_1}$ ³ may also help in improving the significance slightly. We have chosen a minimum cut of 55 GeV on $p_T^{l_2}$ and a minimum cut of 1.8 on the angle $\Delta\phi_{\cancel{E}_T, l_1}$ in our present analysis. With the help of these optimal values of cuts, a signal significance of about 4.6 can be achieved assuming an integrated luminosity $L = 3000 \text{ fb}^{-1}$, for the case of $M_{H^\pm} = 150 \text{ GeV}$.

Cuts applied	No of events		S/B	Significance (S_σ)
	H^+H^- (S)	W^+W^- (B)		
	$M_{H^\pm}=150$ (200) GeV		$M_{H^\pm}=150$ (200) GeV	$M_{H^\pm}=150$ (200) GeV
Initial Signal	2331.8 (855.3)	931500.0	0.002 (0.001)	2.3 (0.9)
Isolation + 0j	943.7 (321.3)	431865.4	0.002 (0.001)	1.4 (0.5)
Acceptance cut	739.5 (263.9)	288626.8	0.002 (0.001)	1.4 (0.5)
$\cancel{E}_T > 110 \text{ GeV}$	201.6 (107.9)	7423.1	0.028 (0.014)	2.3 (1.2)
$\Delta\phi_{\cancel{E}_T, l_2} > 1.6$	40.0 (33.5)	292.1	0.130 (0.115)	2.3 (1.9)
$p_T^{l_2} > 55 \text{ GeV}$	8.6 (13.6)	1.9	4.382 (7.301)	4.3 (6.2)
$\Delta\phi_{\cancel{E}_T, l_1} > 1.8$	8.5 (13.5)	1.5	5.415 (9.020)	4.6 (6.5)

TABLE III. Cut flow table at 14 TeV center-of-mass energy and 3000 fb^{-1} integrated luminosity for $M_{H^\pm} = 150 \text{ GeV}$ and 200 GeV . The significance (S_σ) is defined in Eq. 11.

The effects of applying various cuts on the signal and background events have been summarized as a cut flow scheme in Table III for the two benchmark values of the charged Higgs mass of 150 GeV and 200 GeV. We have selected only those cuts that increase the signal significance (S_σ) defined as

$$S_\sigma = \sqrt{2(S+B)\ln(1+S/B) - 2S}, \quad (11)$$

where S and B are number of signal and background events respectively. This significance estimator is useful for events with low statistics [26]. When the background is large, the formula for S_σ reduces to the more familiar S/\sqrt{B} form used for estimating the signal significance. Although the number of events that satisfy all the applied cuts are low, the

³ Angle between the missing energy and the leading lepton in the transverse plane

significance is nevertheless promising. With the 3000 fb^{-1} integrated luminosity, the same set of cuts lead to a signal significance of about 6.5 for $M_{H^\pm} = 200 \text{ GeV}$. We can further improve the significance by optimizing various cuts. For example, pushing the minimum \cancel{E}_T cut on the higher side does help in achieving better significance. As mentioned before, a suitable large cut on M_{eff} instead of the cut on $p_T^{l_2}$ can also be used to suppress the background efficiently. However, in that case the minimum \cancel{E}_T cut should be relaxed slightly to maintain a high signal significance.

As both $\Delta\phi_{\cancel{E}_T, l_2}$ and $p_T^{l_2}$ play an important role in enhancing the signal significance, it will be useful to study a possible correlation between the minimum cuts that can be applied on these kinematic variables. We have shown this correlation in Fig. 7 using the contour plots for $M_{H^\pm}=150, 200 \text{ GeV}$. The plots are shown for two values of the integrated luminosity, *viz* $L = 3000 \text{ fb}^{-1}$ and $L = 5000 \text{ fb}^{-1}$. The contour plots have been obtained after applying the minimum $\cancel{E}_T > 110 \text{ GeV}$ cut along with the acceptance cuts. In these plots we show the minimum cuts on $p_T^{l_2}$ and $\Delta\phi_{\cancel{E}_T, l_2}$ required to achieve a signal significance $S_\sigma \geq 2$, keeping the total number of events $S+B \geq 5$. The signal significance is clearly seen to increase substantially with more optimal choices of cuts for the two correlated kinematic variables. The variation in the signal significance is represented with different color codes. With the help of these plots it is easier to find the optimal values of the cuts on $\Delta\phi_{\cancel{E}_T, l_2}$ and $p_T^{l_2}$ which can maximize the significance. We should also point out that our analysis for the two benchmark values of the charged Higgs mass achieved a signal significance in accordance with the contour plots shown in Fig. 7a and 7b. However, the efficiency of these correlated cuts for the case of $M_{H^\pm} = 200 \text{ GeV}$ which is clearly visible in Fig. 7b, suggests that a significance, as high as 5σ , should be well within the reach with more optimal choices of the cuts when compared to those listed in Table III. As expected, with higher integrated luminosity, much better signal significance can be achieved (see Figs. 7c and 7d). It is worth pointing out that in Fig. 7, the constraint $S+B \geq 5$ plays a major role in modifying the shape of common significance contours. As the discrete cut-off for events will not be uniform for both $L = 3000 \text{ fb}^{-1}$ and $L = 5000 \text{ fb}^{-1}$, it gives an impression of a non trivial scaling at different luminosities.

In Fig. 8, we estimate the signal significance for various charged Higgs masses assuming 1000, 3000 and 5000 fb^{-1} integrated luminosities at the LHC with $\sqrt{s} = 14 \text{ TeV}$. We have

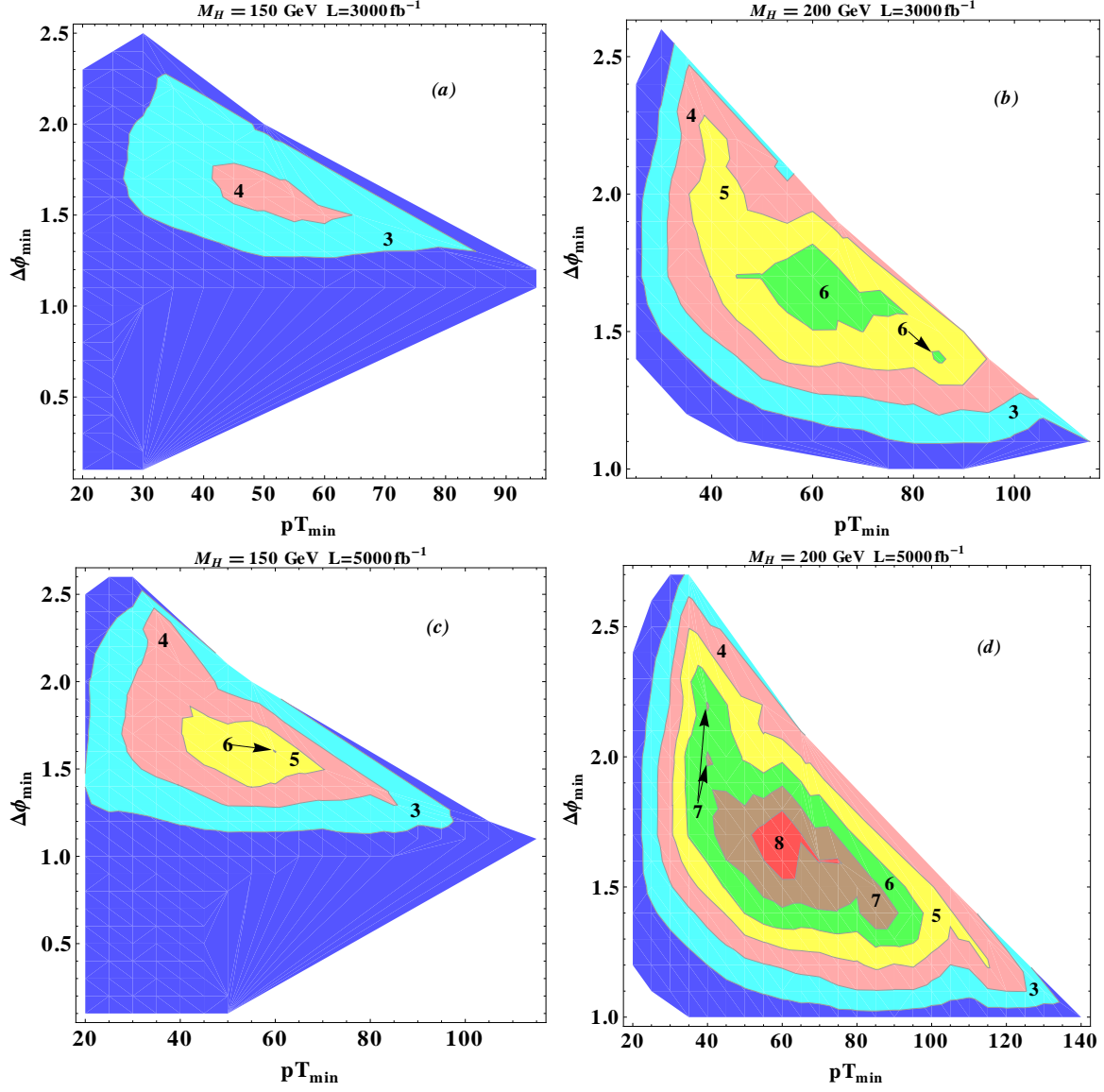


FIG. 7. Contour plots for the significance (S_σ) as a function of minimum cuts on $\Delta\phi_{\cancel{E}_T, l_2}$ (y-axis) and $p_T^{l_2}$ (x-axis) for (a) $M_{H^\pm} = 150$ GeV, $L = 3000 \text{ fb}^{-1}$, (b) $M_{H^\pm} = 200$ GeV, $L = 3000 \text{ fb}^{-1}$, (c) $M_{H^\pm} = 150$ GeV, $L = 5000 \text{ fb}^{-1}$, and, (d) $M_{H^\pm} = 200$ GeV, $L = 5000 \text{ fb}^{-1}$. The blue shaded regions in the above plots refer to 2σ statistical significance.

applied the same set of cuts as listed in Table III. Since we have applied a large missing energy cut, the significance increases for higher charged Higgs masses. However, beyond a certain value of charged Higgs mass, the significance goes down. This is mainly due to the small pair production cross section of the charged Higgs. We note that for $M_{H^\pm} = 180$

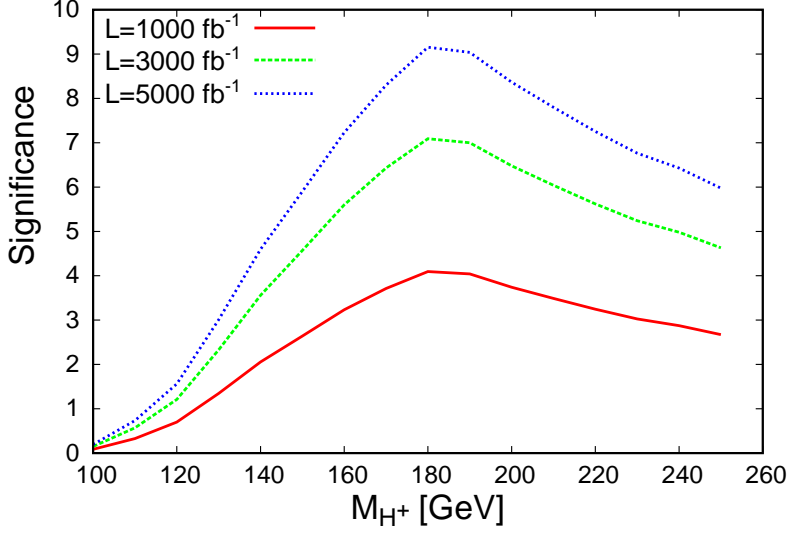


FIG. 8. Illustrating the signal significance for different charged Higgs masses and integrated luminosities. The kinematic cuts are the same as given in Table III.

GeV the significance is seen to become maximum in Fig. 8. This is just the artifact of the choice of \cancel{E}_T cut, which is more effective at that charged Higgs mass. Note that beyond the charged Higgs mass of about 180 GeV, the $H^\pm \rightarrow W^\pm \rho$ decay channel is also open for $M_\rho = 100$ GeV. This reduces the charged Higgs branching ratio in the $W\sigma$ decay mode and hence reduces the signal cross section further for $M_{H^\pm} > 180$ GeV. The upper bound on M_ρ which is related to an upper bound on the coupling λ_5 can be about 470 GeV [4]. It means, by considering heavier ρ mass we can ensure a 100% branching ratio of the charged Higgs decay to $W^\pm \sigma$ for the heavier charged Higgs masses. It is needless to say that optimization of kinematic cuts is required to estimate the actual signal significance for different charged Higgs masses. For example, despite larger signal cross section for $M_{H^\pm} = 120$ GeV, the significance is maximized for a minimum \cancel{E}_T cut of 90 GeV. On the other hand, for $M_{H^\pm} = 220$ GeV we have smaller signal cross section but a minimum cut of 130 GeV on \cancel{E}_T is more helpful in achieving a larger signal significance. We note that $(\Delta\phi_{\cancel{E}_T, l_2}, p_T^{l_2})$ combination which we have used to discriminate the signal from the background for $M_{H^\pm} = 150, 200$ GeV is not very useful in increasing the significance for lower M_{H^\pm} values. This is related to the fact that the efficiency of these cuts is closely related to the high \cancel{E}_T cut which in turn is related to the mass difference between the

charged Higgs and the W boson. When the mass difference between the charged Higgs and the W boson is not large enough, the application of high \cancel{E}_T cut also kills the signal along with the background. It is also worth pointing out that for larger charged Higgs masses a suitable $\Delta\phi_{\cancel{E}_T, l_2}$ cut with large enough \cancel{E}_T cut is sufficient. In other words, if it is possible to apply a very high \cancel{E}_T cut, the additional $p_T^{l_2}$ cut becomes less relevant.

VI. SUMMARY AND CONCLUSION

We have studied the signatures of charged Higgs boson at the LHC in a two Higgs doublet model with right-handed neutrinos. The model, aiming to derive neutrino masses via preferential Yukawa couplings $\mathcal{O}(1)$ with an additional Higgs doublet, also implies large Yukawa coupling of the charged Higgs with the light leptons and neutrinos. However, if cosmological constraints are taken into account, the leptonic decay mode of the charged Higgs is highly suppressed and $H^\pm \rightarrow W^\pm \sigma$ is the dominant decay mode. In this study, the charged Higgs pair production via the Drell-Yan process and its further decay leading to opposite sign di-leptons+missing energy in the final state is considered as the signal. The major SM background to the signal comes from the process, $pp \rightarrow W^+W^-$. We have done a complete signal-background cut based analysis for both the 8 TeV and 14 TeV center-of-mass energies at LHC. The charged Higgs masses of 150 GeV and 200 GeV serve as the benchmark points for our study. Since the signal has additional sources of missing energy, we find that a large \cancel{E}_T cut helps in suppressing the SM background. Also, a combination of minimum cuts on the angle $\Delta\phi_{\cancel{E}_T, l_2}$ and $p_T^{l_2}$ plays an important role in enhancing the signal significance. Due to the lack of sufficient data and the low signal cross section as compared to the background, the observability of the signal is not possible at the LHC with $\sqrt{s} = 8$ TeV and we therefore carry out our analysis for the 14 TeV run of the LHC. We find that even at the 14 TeV run of LHC, a charged Higgs with the characteristics of a “fermiophobic” field will prove elusive without a very optimized kinematic selection of events even with high integrated luminosity. We show this by identifying the kinematic variables sensitive to specific selection cuts which with a large (3000 fb^{-1}) integrated luminosity yields a signal significance of 4.6σ for $M_{H^\pm} = 150$ GeV. For the case of $M_{H^\pm} = 200$ GeV, a signal significance of 5σ can be easily achieved with better statistics. We highlight

the significance of the optimized cuts in the analysis through a correlation plot for event selection that enhances the signal significance in a very robust way. Our analysis indicates that the observation of this otherwise elusive fermiophobic charged Higgs boson is quite promising at the high energy and high luminosity run of the LHC, provided a proper event selection criterion is applied.

ACKNOWLEDGMENTS

We thank Arindam Chatterjee and Sandhya Choubey for fruitful discussions. The work of UM, BM, SKR and AS was partially supported by funding available from the Department of Atomic Energy, Government of India, for the Regional Centre for Accelerator-based Particle Physics, Harish-Chandra Research Institute. The work of SN was supported in part by the U.S. Department of Energy Grant Number DE-SC0010108.

-
- [1] G. Aad *et al.* [ATLAS Collaboration], Phys. Lett. B **716**, 1 (2012); S. Chatrchyan *et al.* [CMS Collaboration], Phys. Lett. B **716**, 30 (2012).
 - [2] M. C. Gonzalez-Garcia and Y. Nir, Rev. Mod. Phys. **75**, 345 (2003) [hep-ph/0202058].
 - [3] E. Ma, Phys. Rev. Lett. **86**, 2502 (2001) [hep-ph/0011121].
 - [4] S. Gabriel and S. Nandi, Phys. Lett. B **655**, 141 (2007) [hep-ph/0610253].
 - [5] F. Wang, W. Wang and J. M. Yang, Europhys. Lett. **76**, 388 (2006) [hep-ph/0601018].
 - [6] S. M. Davidson and H. E. Logan, Phys. Rev. D **80**, 095008 (2009) [arXiv:0906.3335 [hep-ph]];
 - [7] S. Gabriel, B. Mukhopadhyaya, S. Nandi and S. K. Rai, Phys. Lett. B **669**, 180 (2008) [arXiv:0804.1112 [hep-ph]].
 - [8] S. M. Davidson and H. E. Logan, Phys. Rev. D **82**, 115031 (2010) [arXiv:1009.4413 [hep-ph]].
 - [9] G. C. Branco, P. M. Ferreira, L. Lavoura, M. N. Rebelo, M. Sher and J. P. Silva, Phys. Rept. **516**, 1 (2012) [arXiv:1106.0034 [hep-ph]] and the references there in.
 - [10] S. Zhou, Phys. Rev. D **84**, 038701 (2011) [arXiv:1106.3880 [hep-ph]]; M. Sher and C. Triola, Phys. Rev. D **83**, 117702 (2011) [arXiv:1105.4844 [hep-ph]].

- [11] R. N. Mohapatra and G. Senjanovic, Phys. Rev. Lett. **44**, 912 (1980) and the references there in.
- [12] Z. Maki, M. Nakagawa and S. Sakata, Prog. Theor. Phys. **28**, 870 (1962); B. Pontecorvo, Sov. Phys. JETP **26**, 984 (1968) [Zh. Eksp. Teor. Fiz. **53**, 1717 (1967)].
- [13] G. L. Fogli, E. Lisi, A. Marrone, D. Montanino, A. Palazzo and A. M. Rotunno, Phys. Rev. D **86**, 013012 (2012) [arXiv:1205.5254 [hep-ph]].
- [14] G. Steigman, K. A. Olive and D. N. Schramm, Phys. Rev. Lett. **43**, 239 (1979); K. A. Olive, G. Steigman and T. P. Walker, Phys. Rept. **333**, 389 (2000) [astro-ph/9905320].
- [15] P. A. R. Ade *et al.* [Planck Collaboration], arXiv:1303.5062 [astro-ph.CO]; P. A. R. Ade *et al.* [Planck Collaboration], arXiv:1303.5076 [astro-ph.CO]; C. L. Bennett *et al.* [WMAP Collaboration], Astrophys. J. Suppl. **208**, 20 (2013) [arXiv:1212.5225 [astro-ph.CO]].
- [16] ATLAS Collaboration conference note [ATLAS-CONF-2013-011].
- [17] CMS Collaboration [CMS-PAS-HIG-13-028].
- [18] J. Beringer *et al.* (Particle Data Group), Phys. Rev. D **86**, 010001 (2012).
- [19] J. Pumplin, D. R. Stump, J. Huston, H. L. Lai, P. M. Nadolsky and W. K. Tung, JHEP **0207**, 012 (2002) [hep-ph/0201195].
- [20] J. Alwall, M. Herquet, F. Maltoni, O. Mattelaer and T. Stelzer, JHEP **1106**, 128 (2011) [arXiv:1106.0522 [hep-ph]].
- [21] N. D. Christensen and C. Duhr, Comput. Phys. Commun. **180**, 1614 (2009) [arXiv:0806.4194 [hep-ph]].
- [22] <https://cp3.irmp.ucl.ac.be/projects/madgraph/wiki/FAQ-General-13>
- [23] T. Sjostrand, S. Mrenna and P. Z. Skands, Comput. Phys. Commun. **178**, 852 (2008) [arXiv:0710.3820 [hep-ph]].
- [24] G. Aad *et al.* [ATLAS Collaboration], Phys. Rev. D **87**, 112001 (2013) [arXiv:1210.2979 [hep-ex]].
- [25] G. Aad *et al.* [ATLAS Collaboration], arXiv:0901.0512 [hep-ex]; Bruce Mellado, Private Communication.
- [26] G. Cowan, K. Cranmer, E. Gross and O. Vitells, Eur. Phys. J. C **71**, 1554 (2011) [arXiv:1007.1727 [physics.data-an]].